J. Phys.: Condens. Matter **23** (2011) 416003 (9pp) doi:10.1088/0953-8984/23/41/416003

Persistence of magnons in a site-diluted dimerized frustrated antiferromagnet

M B Stone[1], A Podlesnyak[1], G Ehlers[1], A Huq[1], E C Samulon[2,3], M C Shapiro[2,3] and I R Fisher[2,3]

[1] Neutron Scattering Science Division, Oak Ridge National Laboratory, Oak Ridge, TN 37831, USA
[2] Geballe Laboratory for Advanced Materials and Department of Applied Physics, Stanford University, Stanford, CA 94305, USA
[3] Stanford Institute of Energy and Materials Science, SLAC National Accelerator Laboratory, 2575 Sand Hill Road, Menlo Park, CA 94025, USA

E-mail: stonemb@ornl.gov

Received 8 June 2011, in final form 31 August 2011
Published 28 September 2011
Online at stacks.iop.org/JPhysCM/23/416003

Abstract
We present inelastic neutron scattering and thermodynamic measurements characterizing the magnetic excitations in a disordered spin-liquid antiferromagnet with non-magnetic substitution. The parent compound $Ba_3Mn_2O_8$ is a dimerized, quasi-two-dimensional geometrically frustrated quantum disordered antiferromagnet. We substitute this compound with non-magnetic V^{5+} for the $S = 1$ Mn^{5+} ions, $Ba_3(Mn_{1-x}V_x)_2O_8$, and find that the singlet–triplet excitations which dominate the spectrum of the parent compound persist for the full range of substitution examined, up to $x = 0.3$. We also observe additional low-energy magnetic fluctuations which are enhanced at the greatest substitution values.

(Some figures in this article are in colour only in the electronic version)

1. Introduction

Dimerized quantum disordered antiferromagnets (AFMs) serve as clean systems for experimentally testing theoretical models [1–4]. One approach to study these systems is to initially characterize the quantum ground state and its excitations, and then explore emergent phenomena by perturbing the system via external tunable parameters. One can then examine how these parameters change the intrinsic dynamics of the system. Besides temperature, clean external parameters available to modify the ground state of such systems include applied magnetic fields [5–7], and hydrostatic and uniaxial pressure [8–11]. One other approach to modifying the quantum states of these systems is to chemically perturb the Hamiltonian via magnetic or non-magnetic substitution [12–15].

Doping or substitution dependent experimental studies of AFMs have primarily used thermodynamic measurements to examine the creation of or the change in ordering temperature of a long range magnetically ordered phase. In the case of the spin-Peierls (SP) compound $CuGeO_3$, the SP temperature decreases with initial substitution, and eventually a long range ordered AFM phase develops with further substitution of magnetic sites [16]. The development of long range magnetic order and its temperature dependence for substitution on the magnetic site has also been examined in several systems with disordered ground states and a finite energy-gap or spin-gap to excitations. These include the quantum spin ladder $Sr(Cu_{1-x}Zn_x)_2O_3$ [17], the Haldane chain $Pb(Ni_{1-x}Mg_x)_2V_2O_8$ [18], and the coupled quantum dimer system $TlCu_{1-x}Mg_xCl_3$ [19]. In these examples it is proposed that diluting the magnetic sites creates effective unpaired spins, i.e. local moments, in the vicinity of the non-magnetic substituted site. This can be understood considering a simple broken spin dimer. These local moments may modify the interactions enough such that long range magnetic order becomes the new magnetic ground state of the system in what has been termed an 'order by disorder' transition [20–22].

The spin dimer compound $Ba_3Mn_2O_8$ provides a new context in which to explore the consequences of non-magnetic substitution. $Ba_3Mn_2O_8$ is an AFM composed of $S = 1$ $3d^2$ Mn^{5+} spin pairs or dimers arranged vertically on a hexagonal lattice [23]. Figures 1(a) and (b) illustrate the

crystal structure and intradimer and interdimer exchange interactions [23, 24]. Hexagonal layers of dimers are separated from one another along the crystallographic c-axis by 12-fold oxygen coordinated Ba sites. Initial thermodynamic measurements characterized the spin-gap and a number of nearest neighbors weighted sum of exchange constants [25–27]. These measurements indicated that the magnetic ground state of $Ba_3Mn_2O_8$ is a non-magnetic singlet phase; the AFM dimer excitations are from the $S = 0$ singlet ground state to the $S = 1$ triplet and $S = 2$ quintet states. Previous INS measurements of powders and single crystals directly showed the propagating triplet modes of the coupled dimers and determined the significant exchange interactions and their magnitude [28, 24, 29]. These measurements found that the intra- and inter-layer exchange enhances the two-dimensional (2D) nature of the magnetic lattice. There are also two low-temperature high field regions of long range magnetic order in $Ba_3Mn_2O_8$. These are essentially field-induced condensates of the triplet and quintet states of the dimer network. The value of the spin-gaps, singlet–triplet $\Delta \approx 1$ meV and singlet–quintet $\Delta \approx 3.4$ meV, allows one to experimentally access both critical fields of these phases [27, 25, 30, 26]. The influence of the zero-temperature quantum critical point (QCP) on thermodynamic parameters has also been measured in detail [26].

Substitution of $S = 0$, $3d^0$, V^{5+} for $S = 1$, $3d^2$, Mn^{5+} is possible, and the solid solution $Ba_3(Mn_{1-x}V_x)_2O_8$ is available for $0 \leq x \leq 1$. Because the vanadium and manganese ions have the same valence, no charge is added to the system. Substitution of non-magnetic ions breaks the singlet dimers. This also affects the excited triplet band and creates $S = 1$ Mn moments. These moments are not as strongly exchange coupled as those of the $x = 0$ dimers. The magnetic ground state of the system is thus modified. In a recent study, Samulon *et al* have investigated the thermodynamic response of single crystals of this non-magnetic substituted system at low temperatures for $x < 0.05$ [31]. They observe no signature of a transition to long range magnetic order down to temperatures as low as 50 mK. Magnetic entropy is slowly recovered over a fairly wide temperature window, but the composition and temperature dependence of the heat capacity do not conform to expectations for spin glass behavior, leading to the suggestion that the material exhibits random singlet formation at low temperatures. Within such a scenario, Mn ions on unbroken dimers form singlet pairs, as for the parent compound, with an energy scale set by the intradimer exchange J_0. Unpaired Mn moments associated with broken dimers are nevertheless exchange coupled, and pairs of moments with the largest exchange interaction form singlets as the temperature is progressively reduced. As temperature further decreases this process continues until there exists a distribution of weak exchange coupled singlets, i.e. a random singlet phase, existing within the sea of strongly coupled dimers of the unsubstituted compound. Such a ground state is favored by the hierarchy of exchange coupling in the $Ba_3Mn_2O_8$ lattice, and indeed the observed heat capacity can be reasonably well accounted for by a simplified model for random singlet formation using the bare exchange constants of the parent compound [31].

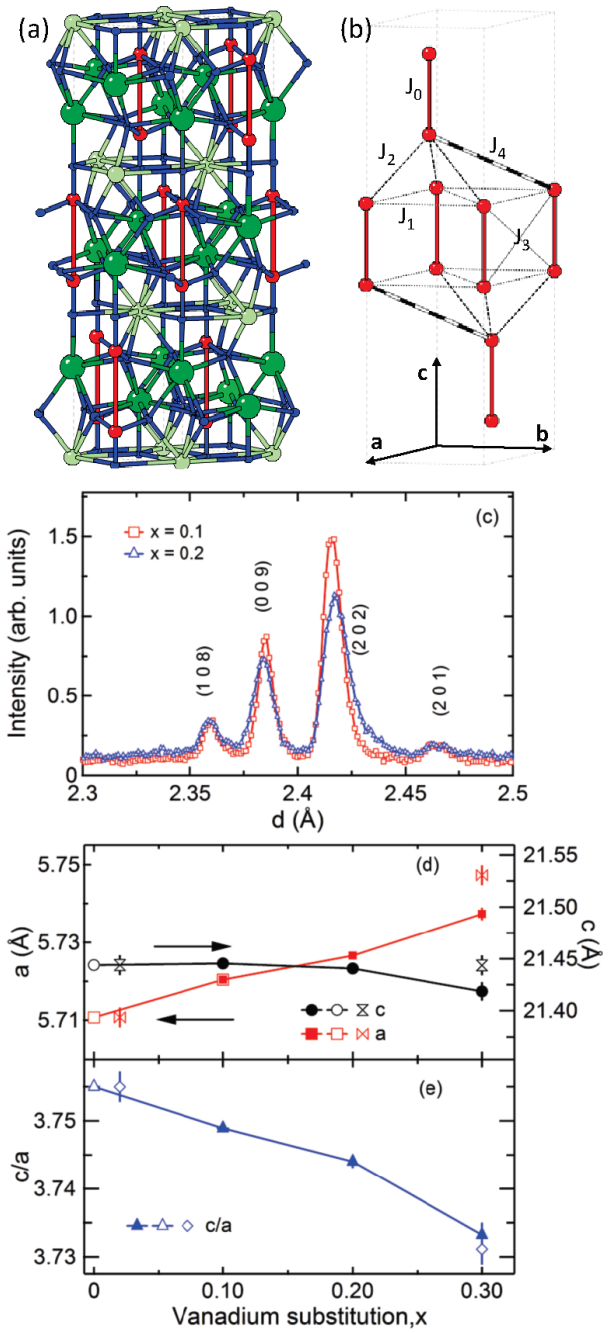

Figure 1. (a) Crystal structure of $Ba_3Mn_2O_8$ [23]. Small red circles represent Mn atoms, medium light green circles and large dark green circles represent Ba atoms (12-fold and 10-fold coordinated respectively), and tiny blue circles represent oxygen atoms. (b) Mn^{5+} magnetic ions and the significant exchange interactions found for $Ba_3(Mn_{1-x}V_x)_2O_8$ [24]. (c) Neutron powder diffraction intensity as a function of d-spacing for two values of x. Indices of Bragg peaks are indicated for the peaks shown. (d) a and c lattice constants as a function of vanadium substitution in $Ba_3(Mn_{1-x}V_x)_2O_8$. Open symbols for $x = 0$ are literature [23] values. Open symbols for $x = 0.02$ and 0.3 are from laboratory x-ray measurements. Vertical axis ranges were chosen to display lattice constants over the same range of $\Delta a/a$ as $\Delta c/c$. (e) c/a ratio as a function of vanadium substitution. Lattice constants were refined from time-of-flight neutron powder diffraction measurements (solid symbols) as described in the text. Error bars of neutron scattering data are shown as the standard deviation multiplied by five times the reduced chi squared value of the refinement. Measurements were performed at room temperature.

In this paper, we present inelastic neutron scattering (INS) measurements that directly probe the magnetic excitations of $Ba_3(Mn_{1-x}V_x)_2O_8$. We find that the dimer excitations of the parent compound remain remarkably stable even for the greatest levels of substitution examined. Such excitations have also been directly probed in other chemically substituted systems using INS. Though, a long range ordered phase is very often also observed [32, 13, 33]. Our measurements indicate no sign of a transition to short or long range magnetic order down to $T = 1.8$ K, even for the highest concentrations studied ($x = 0.3$). One of the most dramatic changes in the spectrum is the appearance of low-energy fluctuations for the greatest levels of substitution. As the dimer singlet–triplet (i.e. triplet) excitations are depopulated with non-magnetic substitution, these additional low-energy fluctuations increase in number. These excitations are consistent with the high-temperature manifestation of excitations out of a random singlet phase.

2. Experimental methods

Powder samples of $Ba_3(Mn_{1-x}V_x)_2O_8$ were synthesized via solid state reaction following the procedure described for $Ba_3Mn_2O_8$ [28, 27]. Powder samples were produced for $x = 0$, 0.02, 0.05, 0.2, 0.3. Stoichiometric amounts of $BaCO_3$, Mn_2O_3 and V_2O_5 were calcined under flowing oxygen at 900 °C for 30 h, and the resulting powder was reground and sintered in temperatures up to 1050 °C for 70 h. $x = 0.02$ and 0.3 samples were examined for phase purity using a laboratory Cu anode x-ray powder diffractometer. No additional phases or unreacted materials were observed for V concentrations of $x = 0.02$ and 0.3. All powder samples were prepared using the same procedure. Powder samples were used for inelastic neutron scattering measurements in order to quickly measure large portions of energy and wavevector transfer space in a series of samples, and because significant quantities of single crystals were not available.

Low field magnetic DC susceptibility measurements were performed on powder samples using a commercial SQUID magnetometer. Measurements were performed between $T = 1.8$ and 300 K in an applied magnetic field of $\mu_0 H = 0.1$ T. The magnetic susceptibility was determined by dividing the magnetization, M, by the applied magnetic field, $\chi = M/\mu_0 H$. No phase transitions associated with potential metal oxide impurity phases were observed in any of the samples.

High resolution neutron powder diffraction measurements were performed for a range of substitution. These were performed using the Powgen time-of-flight diffractometer at the Spallation Neutron Source (SNS). Diffraction patterns were acquired on powder samples at room temperature. Samples consisted of approximately 2 g of powder contained in vanadium sample cans. Samples were measured for approximately 2.5 h using 1.066 Å wavelength neutrons.

Inelastic neutron scattering spectra were measured using the cold neutron chopper spectrometer (CNCS) instrument at the SNS [49]. Spectra were acquired using powder samples in aluminum sample cans under He exchange gas. The sample environment consisted of a He-flow cryostat. A cadmium mask was applied directly to the aluminum sample can to reduce multiple scattering and aluminum scattering from the cryostat. The powder samples were measured with $E_i = 3.2$ meV incident energy neutrons using the standard resolution configuration of the instrument. This yielded a full width at half maximum (FWHM) elastic energy resolution of 0.0736(5) meV as[4] determined from the incoherent elastic scattering of a vanadium standard. Sample masses for different substitution values were each approximately 5 g. The data were individually normalized to the calculated moles of Mn^{5+} spin in each sample[5].

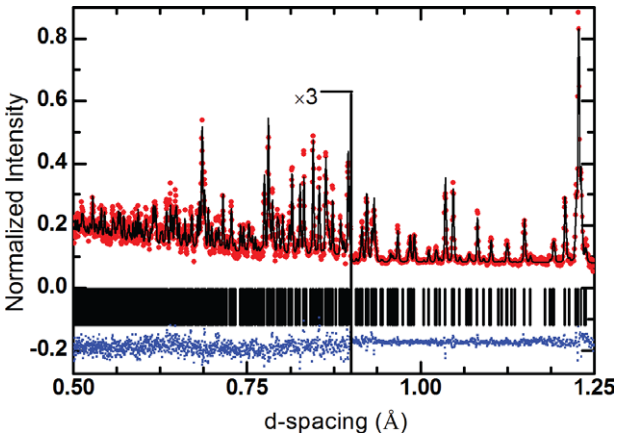

Figure 2. Rietveld refinement of $Ba_3(Mn_{1-x}V_x)_2O_8$ for $x = 0.2$. Red circles are the measured scattering intensity. Solid black line is the refined diffraction pattern as described in the text. Solid vertical lines represent the location of individually indexed Bragg reflections. Blue squares at the bottom of the figure represent the difference in measured and refined scattering intensity. Data were measured at room temperature using the Powgen instrument. Refinement details are described in the text.

3. Results

We have characterized the crystal structure of three different substitution values for $Ba_3(Mn_{1-x}V_x)_2O_8$, $x = 0.1$, 0.2, 0.3, via powder neutron diffraction. We observe no sign of a structural phase transition as a function of vanadium doping. Figure 2 shows the measured scattering intensity for the $x = 0.2$ sample as a function of d-spacing. Figure 1(c) shows a small portion of these diffraction data as a function of d-spacing. There is a small but clear shift in lattice constants as a function of doping. We refined the diffraction data both fixing the atomic positions of all but the Mn and V sites based upon the $x = 0$ structure, and allowing these positions to vary [34]. The quality of refinement did not improve when the atomic positions were allowed to vary. An example of the refined diffraction measurement is shown as a solid line in figure 2. The refined lattice constants are shown in figures 1(d) and (e) as a function of vanadium

[4] Values in parentheses and error bars shown in figures are the standard deviation.

[5] We estimate the potential systematic error in this normalization to be between 10 and 20%. This error is not explicitly included in the presented data or extracted parameters.

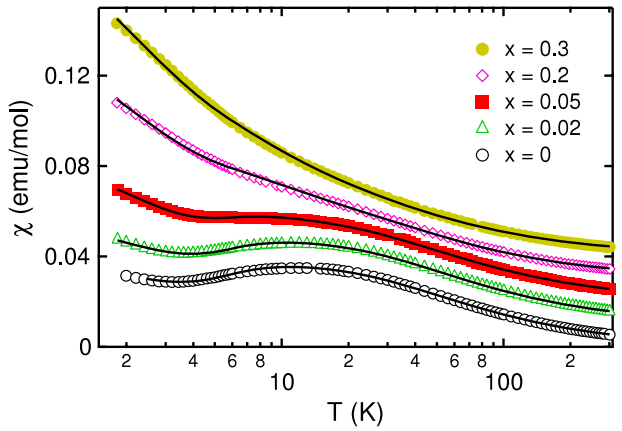

Figure 3. Magnetic susceptibility as a function of temperature for different concentrations of vanadium in $Ba_3(Mn_{1-x}V_x)_2O_8$. Data are normalized per mole of Mn spin. Solid lines are individual fits to a correlated spin (Curie–Weiss) plus $S = 1$ dimer model as described in the text. Data have been offset vertically in multiples of 0.01 emu mol^{-1} for presentation.

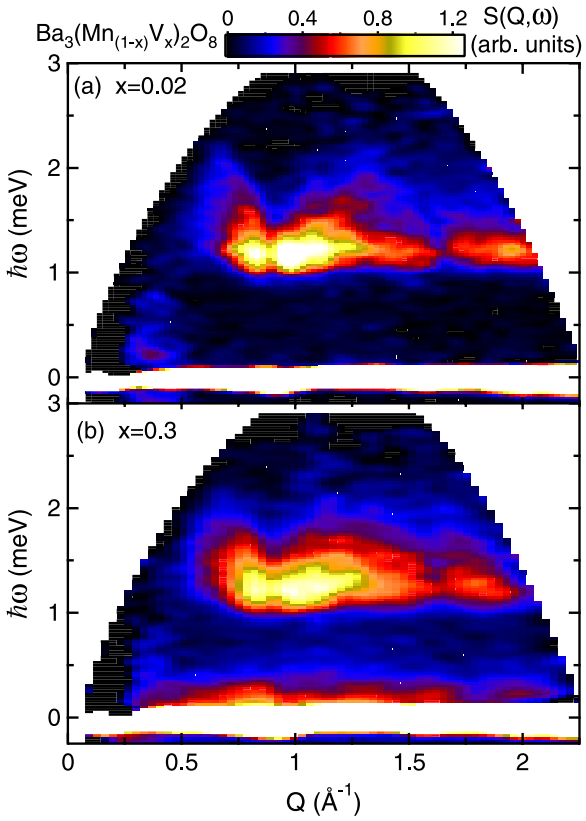

Figure 4. Inelastic neutron scattering intensity as a function of energy and wavevector transfer for $Ba_3(Mn_{1-x}V_x)_2O_8$ with (a) $x = 0.02$ and (b) $x = 0.3$. Data were acquired at $T = 1.8$ K with 3.1 meV incident energy neutrons.

substitution. For comparison, we also show the literature $x = 0$ values from [23]. For small x, the results agree very well with the literature values. As the vanadium doping increases, the a lattice constant slowly lengthens, the c axis gets shorter, and the ratio c/a becomes smaller. Laboratory x-ray measurements were performed for $x = 0.02$ and 0.3. These data are also shown in figures 1(d) and (e). No change in lattice constant was observable from the x-ray measurements for the $x = 0.0$ doping level. The trend as a function of vanadium substitution agrees well with the room temperature lattice constants determined for $Ba_3V_2O_8$: $a = 5.7733(14)$, $c = 21.339(10)$ and $a = 5.7714(9)$, $c = 21.2480(30)$ from [35] and [36] respectively. The overall changes in lattice constant are small as a function of substitution: less than half a per cent for the a-axis and less than 0.1% for the c-axis. This implies that the exchange constants between Mn^{5+} sites are of a very similar magnitude for all samples in this range of vanadium substitution. Consequently, any effects observed in the magnetic properties will be primarily due to intrinsic effects of non-magnetic substitution and not due to changes in exchange constants due to changes in the crystal structure. Although our structural refinement was performed only for room temperature measurements, we find no indication of any structural phase transitions or additional phases in our low-temperature neutron scattering measurements of the magnetic excitations. This was also shown for our prior temperature dependent measurements of the $x = 0$ compound [24, 28].

Figure 3 displays powder magnetic susceptibility as a function of temperature for $Ba_3(Mn_{1-x}V_x)_2O_8$ with $x = 0$, 0.02, 0.05, 0.2, 0.3. The curves for small values of x have a characteristic gradual decrease as temperature is decreased below $T = 20$ K. This is due to the quasi-2D spin-gap phase becoming well defined as the temperature decreases. For the $x = 0$ and $x \leq 0.02$ samples, there is a roll-over at approximately 20 K. As substitution increases, this roll-over is gradually dominated by a rapidly increasing component of the susceptibility at low temperatures. This low-temperature increase is induced by unpaired Mn spins which are created by vanadium sites breaking the spin dimers which define the spin-gap phase at lower temperatures.

Figure 4 illustrates the measured INS spectra for $x = 0.02$ and 0.3 of $Ba_3(Mn_{1-x}V_x)_2O_8$. The $x = 0.02$ data appear nearly identical to the $x = 0$ powder measurements performed previously [28]. There is a single gapped excitation between approximately $\hbar\omega = 1$ and 2.5 meV energy transfer. This is the magnon excitation associated with the transition from the singlet ground state to the triplet of states of the $S = 1$ spin dimers. The intensity is strongly modulated as a function of wave vector transfer, Q, with a peak at $Q = 1$ Å^{-1}. The quasi-2D nature of the exchange coupling in the compound results in a characteristic smeared 'V' in the powder INS spectrum as a function of energy and wavevector transfer. This is still evident in the $x = 0.02$ data in figure 4(a). The $x = 0.3$ data still have this characteristic shape albeit less well defined. The wavevector dependent intensity modulation is nearly identical to that observed for the $x = 0.02$ data. This implies that the strongest exchange interactions are the same between Mn^{5+} moments as in the $x = 0.02$ samples and likewise the $x = 0$ material, i.e. the strong dimer bond is unaffected by non-magnetic substitution. The gap in the spectrum is slightly larger for the $x = 0.3$ sample. The greatest difference in these spectra is the

existence of additional low-energy fluctuations in the $x = 0.3$ sample. These quasi-elastic excitations are localized around elastic energy transfers and generally decrease in intensity as wavevector increases, implying a magnetic origin. In addition from examining the elastic scattering channel, we observe no structural phase transition or transition to AFM long range order as a function of temperature and vanadium substitution.

4. Discussion

We compare the magnetic susceptibility to a simple sum of the spin dimer and free spin contributions:

$$\chi = \frac{C}{T-\Theta} + \frac{\chi_d}{1+\lambda\chi_d} + \chi_0 \tag{1}$$

where

$$\chi_d = \frac{2N\beta g^2\mu_B^2(1+5e^{-2\beta J})}{3+e^{\beta J}+5e^{-2\beta J}}, \tag{2}$$

$$\lambda = \frac{3[J_1+J_4+2(J_2+J_3)]}{Ng^2\mu_B^2} = \frac{3J'}{Ng^2\mu_B^2}, \tag{3}$$

$\beta = \frac{1}{k_B T}$, g is the Lande-g factor, μ_B is the Bohr magneton, N is the number of dimers per mole, and χ_0 is a diamagnetic contribution to the magnetic susceptibility. In equation (1), $(\frac{C}{T-\Theta})$ is a Curie–Weiss law contribution from weakly coupled moments. This is included to describe the low-temperature behavior of unpaired spins associated with the non-magnetic substitution. The second contribution in equation (1) is a mean field expression for the dimer contribution, including the intradimer exchange constant J and interdimer, exchange constants J_1, J_2, J_3 and J_4 [27]. Equation (3) represents a number of nearest neighbors weighted linear sum of the interdimer exchange with the effective exchange J'. An initial fit is performed to the data for the parent compound. We then fix the values of the exchange constants and Lande-g factor determined from the $x = 0$ sample in the magnetic susceptibility fits for the $x \neq 0$ samples. This is reasonable, given the very small change in lattice constants for this range of substitution, and the lack of a significant change to the magnon spectrum defined by the exchange constants J and J'. The lines shown in figure 3 correspond to these fits. These results agree very well with the measurements over a large range of temperature and substitution level. Figure 5(a) shows the variation in the unpaired spin concentration, C from equation (1), as a function of x.

We first characterize the INS measurements of the gapped portion of the magnetic spectrum and then examine the low-energy fluctuations. Our measurements of the $x = 0$ compound found that the wavevector dependent scattering intensity of the triplet excitation agreed very well with the scattering function $\mathcal{S}(\mathbf{Q}, \hbar\omega)$ for isolated spin-1 dimers:

$$\mathcal{S}(\mathbf{Q}, \hbar\omega) = \frac{4e^{2J\beta}[1-\cos(\mathbf{Q}\cdot\mathbf{d})]}{e^{2J\beta}+3e^{J\beta}+5e^{-J\beta}}\delta(\hbar\omega - J). \tag{4}$$

In equation (4), J is the exchange constant of the dimer and $\mathbf{d}$ is the vector between dimer spins. The powder averaged

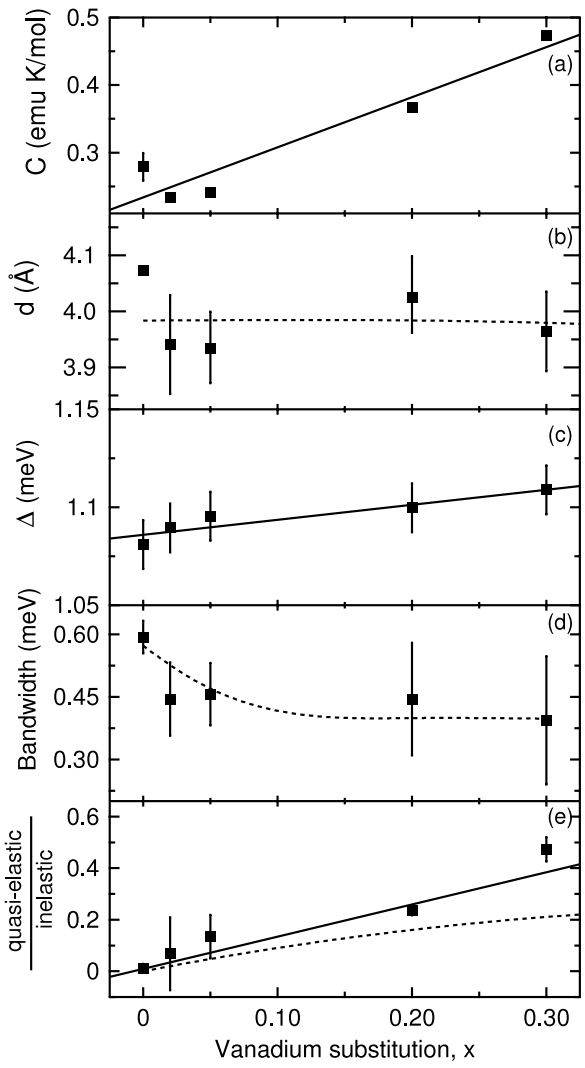

Figure 5. Parameters as a function of vanadium substitution x, of $Ba_3(Mn_{1-x}V_x)_2O_8$: (a) C value determined from low-temperature powder magnetic susceptibility, (b) dimer length d, (c) spin-gap, (d) bandwidth and (e) the ratio of the integrated quasi-elastic scattering intensity to the integrated inelastic scattering intensity. All parameters determined at 1.8 K. Solid lines are fits as described in the text. The dashed line in (b) is the calculated value of d based upon the vanadium substitution dependent lattice constant shown in figure 1(a). The dashed line in (d) is a guide to the eye. The dashed line in (e) is the theoretical fraction of unpaired spins as a function of vanadium substitution.

first frequency moment of the $T = 0$ scattering function yields information regarding the length of the dimer bond d:

$$\hbar\langle\omega\rangle \equiv \int\int_{-\infty}^{\infty} \frac{d\Omega\, d\omega}{4\pi}\hbar\omega(\mathbf{Q})\mathcal{S}(\mathbf{Q}, \hbar\omega)$$
$$\propto |F(Q)|^2\left[1-\frac{\sin(Qd)}{Qd}\right], \tag{5}$$

where $F(Q)$ is the magnetic form factor of the magnetic ion and $\int d\Omega$ is the powder average integral over reciprocal space. The incident energy used for our measurement was chosen to measure energies to the top of the triplet excitation while preserving energy resolution to observe low-energy excitations in the vicinity of the incoherent elastic scattering.

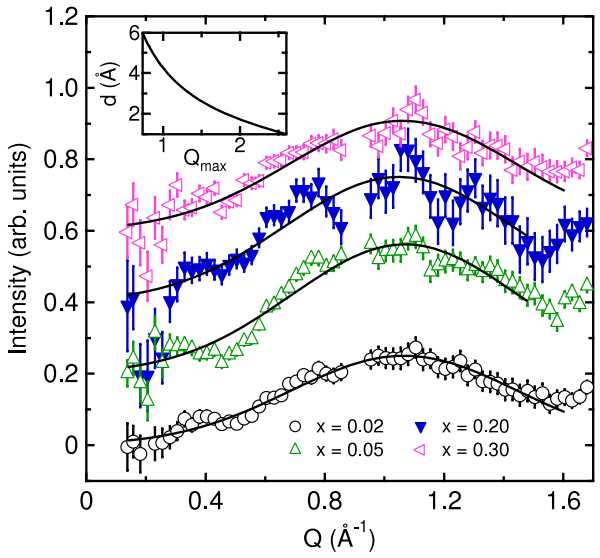

Figure 6. Wavevector dependence of scattering intensity for different vanadium substitutions, x, in $Ba_3(Mn_{1-x}V_x)_2O_8$ for $T = 1.8$ K measurements. Data correspond to integrating over the dimer excitation in the energy range of 0.5 meV $< \hbar\omega <$ 2.9 meV. Data have been offset vertically in multiples of 0.2 units. Solid lines are simple Gaussian fits with a sloping background. Inset shows the distance between dimer pairs plotted against the fitted peak in wavevector transfer for the dimer form factor (equation (5)) discussed in the text.

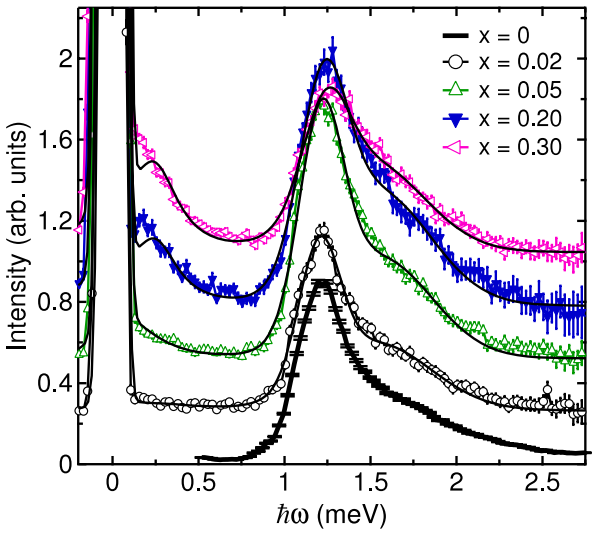

Figure 7. Inelastic neutron scattering intensity as a function of energy transfer for different concentrations of vanadium in $Ba_3(Mn_{1-x}V_x)_2O_8$. Data have been integrated between $Q = 0.6$ and 1.7 Å^{-1}. Data are offset vertically along the y-axis. Solid lines are a parameterization of the elastic scattering and inelastic scattering as described in the text. The $x = 0$ data are reproduced from [28].

The kinematic constraints of this choice limit the range of wavevector transfer, such that only the first maximum of equation (5) is clearly observed in our measurements. In figure 6, we plot the integrated scattering intensity for energy transfers between 0.5 and 2.9 meV for the $T =$ 1.8 K measurements. All of these data have a peak at approximately the same wavevector transfer indicating that the dominant dimer bond is independent of non-magnetic substitution. We numerically calculate the first moment of the spectrum as a function of the dimer length, d, using equation (5). The spin–spin distance d as a function of the value of Q corresponding to the maximum of equation (5) (Q_{max}) is shown as the inset of figure 6. Integrating over the entire triplet mode results in a value which is proportional to the first moment described in equation (5). Because of the limited Q range of the measurement, we perform a simultaneous Gaussian fit to the data in figure 6 using a common background and width for all lineshapes. The corresponding value of d based upon the peak location is plotted in figure 5(b) as a function of x. These values are independent of vanadium substitution and slightly less than that of the parent compound: for vanadium substituted samples the average value of $d = 3.96(4)$ Å while for the previously measured $x = 0$ sample $d = 4.073(7)$ Å [28]. The room temperature value of d based upon the parent compound crystal structure is $d = 3.985$ Å. The dashed line in figure 5(b) is a calculation of the crystallographic d value based upon a smooth interpolation of the c-axis lattice constant data shown in figure 1(d). It is clear that the magnetic dimer contributing to the singlet–triplet excitation in $Ba_3(Mn_{1-x}V_x)_2O_8$ does not change as a function of x.

Figure 7 shows the INS momentum-integrated intensity as a function of energy transfer for the $T = 1.8$ K measurements for different substitution values x. These data are integrated between wavevectors $Q = 0.6$ and 1.7 Å^{-1}. The triplet excitation is the broad peak between 1 meV and approximately 2.5 meV energy transfer. One can also see additional paramagnetic excitations developing at low-energy transfers as the vanadium substitution is increased. INS single crystal measurements for $x = 0$ have very accurately determined the gap, $\Delta = 1.081$ meV, and upper maximum of the dispersion, 2.78 meV [24]. We use these values to parameterize the zero-field data shown in figure 7 by finding the ratio of inelastic intensity to the peak intensity at the spin-gap and maximum dispersion energy transfers. The gap and bandwidth of the vanadium substituted spectra are determined based upon the energy transfers for the intensity ratios of the $x = 0$ data. The spin-gap Δ (simple linear fit shown in figure 5(c)) increases with doping, and the bandwidth decreases slowly with doping (shown in figure 5(d)). As the coupled dimers are substituted non-magnetically, the triplet excitations are no longer able to propagate as freely and the amount of dispersion decreases i.e. approaches the dispersionless isolated dimer limit.

To examine the low-temperature quasi-elastic peaks, we parameterize the energy dependent scattering intensity in figure 7 as a sum of Gaussian and Lorentzian lineshapes. The inelastic triplet excitation is parameterized as a sum of two Gaussians, and the elastic incoherent scattering is parameterized as a single Gaussian peak. The low-energy quasi-elastic scattering is parameterized as a Bose-factor normalized anti-symmetric Lorentzian function (see equation 12 of [28]). This lineshape was then convolved with the energy dependent resolution function of the spectrometer. The ratio of the integrated intensity of the quasi-elastic

scattering to the inelastic scattering is shown in figure 5(e) as a function of x. As substitution increases, the relative amount of quasi-elastic scattering increases. These paramagnetic fluctuations are most likely due to the increasing number of clusters of broken and weakly coupled dimer pairs in the lattice, and reflect the fact that there are several additional relevant interdimer exchange constants in this system. In figure 5(e) the dashed line is the calculated fraction of broken dimer bonds as a function of x. The fraction of quasi-elastic scattering exceeds the number of half magnetically occupied dimers for larger values of vanadium substitution. This indicates that the quasi-elastic scattering is not solely due to broken dimer pairs, but there is likely a contribution from other spin–spin interactions in the lattice. For the range of x examined, the scattering intensity ratio is nearly linear; a linear fit is shown as a solid line in figure 5(e). We also note that a similar linear increase in low-temperature paramagnetic fluctuations was observed in the powder magnetic susceptibility data as illustrated in figure 5(a).

We also examine the temperature dependence scattering of the triplet and quasi-elastic scattering. Figure 8(a) shows the integrated triplet scattering intensity as a function of temperature and vanadium substitution integrated between $0.5\ \text{Å}^{-1} < Q < 1.5\ \text{Å}^{-1}$ and $0.5\ \text{meV} < \hbar\omega < 2.9\ \text{meV}$. We simultaneously fit these data to the temperature dependence described in equation (4) with a common value of dimer exchange, J, and a common constant background. The solid lines in figure 8(a) are the results of this comparison and indicate that this provides a good parameterization of the measured results. The resulting $J = 2.6(2)$ meV is larger than the $x = 0$ value of J_0, but a reasonable approximation of the midpoint of the triplet spectrum. Even at elevated temperatures, the triplet mode of the non-magnetic substituted compound is well approximated by the dimer model.

Figure 8(b) shows the inverse dynamic susceptibility of the quasi-elastic excitation as a function of temperature. The data were integrated between wavevector transfer $0.5\ \text{Å}^{-1} < Q < 1.5\ \text{Å}^{-1}$ and energy transfer $0.25\ \text{meV} < \hbar\omega < 0.5\ \text{meV}$. The integrated intensity was then normalized by the Bose occupation factor, $[1 - \exp(-\hbar\omega/(k_B T))]^{-1}$, using the mean energy transfer of the integrated data to yield the dynamic susceptibility, $\chi_{\text{INS}}(T)$. The inverse dynamic susceptibility increases linearly as a function of temperature for all of the vanadium substitutions of $Ba_3(Mn_{1-x}V_x)_2O_8$ including the $x = 0$ compound, (linear fits are shown in figure 8(b)). This is essentially the Curie–Weiss magnetic susceptibility response of the low-energy magnetic fluctuations. For the inverse susceptibility, the inverse slope is a linear function of the density of moments contributing to the dynamic susceptibility. The slope of the lines decreases with increasing x indicating that as non-magnetic substitution increases, additional magnetic excitations are being populated at lower-energy transfers. This description agrees very well with the measured DC magnetic susceptibility shown in figure 3 and the fitted parameters determined from the low-temperature Curie–Weiss contribution. In figure 8(c), we plot the determined inverse slope of the data in figure 8(b)

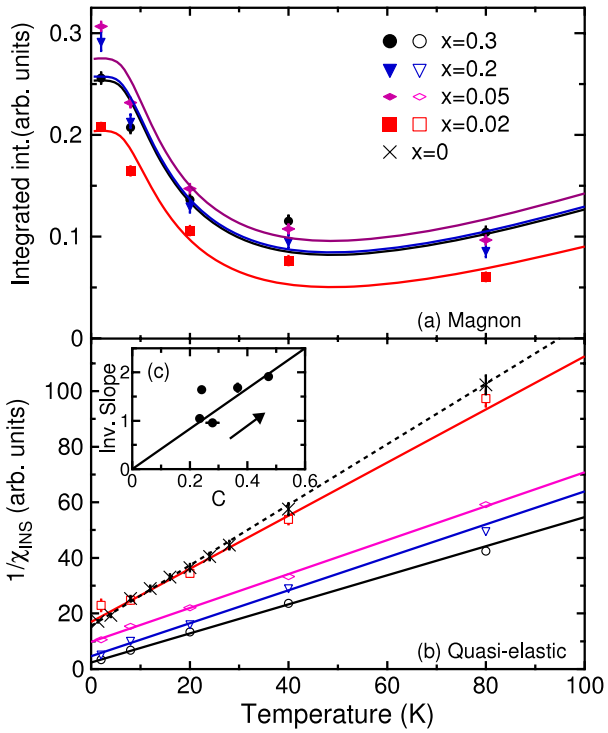

Figure 8. (a) Integrated inelastic scattering intensity as a function of temperature for different vanadium substitutions, x, in $Ba_3(Mn_{1-x}V_x)_2O_8$. Data have been integrated between 0.5 and 1.5 Å^{-1} wavevector transfer for energy transfer $0.5\ \text{meV} < \hbar\omega < 2.9\ \text{meV}$. Solid lines are a global fit to the dimer model described in the text. (b) The Bose-factor normalized inverse scattering intensity of the quasi-elastic scattering intensity for different x in $Ba_3(Mn_{1-x}V_x)_2O_8$ as a function of temperature. Data have been ds integrated between 0.5 and 1.5 Å^{-1} wavevector transfer for energy transfers between 0.25 and 0.5 meV. Solid lines are linear fits described in the text. The dashed line is a linear fit to the $x = 0$ data as described in the text. (c) Inverse slope of the fitted lines shown in panel (b) plotted versus the free spin concentration, C, shown also in figure 5(d). Solid line is a linear fit as described in the text. Arrow indicates the direction of increasing vanadium substitution, x in $Ba_3(Mn_{1-x}V_x)_2O_8$.

as a function of C from the low-temperature Curie–Weiss law fit of the DC magnetic susceptibility in figure 3. The results agree well with one another; a linear fit forced to pass through the origin is shown. The low-energy fluctuations are indeed magnetic in origin. The x-intercepts of the data in figure 8(b) correspond to a Curie–Weiss temperature of the low-energy fluctuations. Although the lack of an absolute normalization of our data does not allow us to accurately determine these values (see footnote 5), we do find they are negative (i.e. AFM) and linearly increasing with vanadium substitution. This is the same trend found for the Curie–Weiss temperature parameter, Θ extracted using equation (1) for the data in figure 3 [31].

The quasi-two-dimensional Shastry–Sutherland [1] frustrated quantum AFM $SrCu_2(BO_3)_2$ [37, 38] has also been examined when non-magnetic Mg sites are substituted for the $S = 1/2$ Cu sites, $SrCu_{2-x}Mg_x(BO_3)_2$ [39, 40]. For this case, single crystal INS measurements found that upon non-magnetic substitution excitations develop below the spin-gap

energy concomitantly with additional excitations within the triplet mode [39]. These effects are described as being due to transitions from the singlet ground state in the presence of a local spin polaron in the presence of a non-magnetic site, to bound states of the triplet and the local spin polaron [41, 42]. This scenario develops in $SrCu_{2-x}Mg_x(BO_3)_2$ due to the high degree of geometrical frustration existing in this layered compound. Our investigation reveals low-energy excitations developing with very little change occurring in the triplet band as a function of non-magnetic substitution in $Ba_3(Mn_{1-x}V_x)_2O_8$. While we cannot rule out the formation of a spin polaron in $Ba_3(Mn_{1-x}V_x)_2O_8$, the reduced energy scale for the new spin excitations, the lack of change to the dynamics of the triplet mode, and the effects observed in thermodynamic measurements [31] are most likely due to a different mechanism. Recently, there have been additional experimental results examining non-magnetic substitution of the Mn^{5+} sites for $Ba_3Mn_2O_8$ [43]. The non-magnetic substituted samples of Manna *et al* were also based upon vanadium substitution with $x = 0.25$, 0.5, 1. Their conclusions for the $x = 0.25$ and 0.5 samples were that substitution diminishes the formation of the AFM dimer and thus eliminates the singlet–triplet excitations. Our INS measurements clearly show otherwise. Rather, the additional quasi-elastic magnetic fluctuations which develop with vanadium doping mask the signature of the singlet–triplet excitations in the magnetic susceptibility measurements for larger values of x.

In contrast to many other non-magnetically substituted gapped systems, no evidence for long range order was found in $Ba_3(Mn_{1-x}V_x)_2O_8$. Instead, vanadium substitution creates additional quasi-elastic excitations. These excitations may be a high-temperature manifestation of a random singlet phase [44–47], as was proposed by Samulon *et al* following their low-temperature thermodynamic studies of this system [31]. Certainly the fact that $Ba_3Mn_2O_8$ has a distribution of exchange energies available to each dimer spin makes this a reasonable possibility. Likewise, the temperature range over which Samulon *et al* observes behavior indicative of a random singlet phase agrees well with the temperature and energy range of our observed quasi-elastic excitations. Susceptibility calculations explicitly show that for temperatures above 2 K the random singlet model is essentially indistinguishable from a Curie susceptibility because the random singlets are only just beginning to form, consistent with our observations. Further high resolution INS measurements performed at lower temperatures using single crystals of intermediate values of x for $Ba_3(Mn_{1-x}V_x)_2O_8$ have the potential to more explicitly determine the nature of the ground state corresponding to the quasi-elastic excitations. Such measurements would also be able to probe the dispersion of the quasi-elastic excitations at low temperatures. Examining the temperature dependence of the low-energy spin-correlations may also provide further characterization of the putative random singlet phase [48].

5. Conclusions

In summary, we have presented results of INS measurements of the site-diluted spin dimer compound $Ba_3(Mn_{1-x}V_x)_2O_8$ in the range $0.05 \leq x \leq 0.3$. Over the entire range studied, the spin-gap associated with the unbroken Mn–Mn dimers remains remarkably robust, with only minor changes reflecting the perturbed triplet dispersion. The existence of a quasi-elastic excitation is shown to be related to the presence of the unpaired spins associated with broken dimers in this system, which for the temperature range studied exhibit an essentially Curie-like susceptibility. These observations are consistent with the proposed random singlet ground state for this system, and motivate more extensive measurements to lower temperatures.

Acknowledgments

MBS thanks M Lumsden, I Zaliznyak, C Batista and B Gaulin for useful discussions. A portion of this research at Oak Ridge National Laboratory's Spallation Neutron Source was sponsored by the Scientific User Facilities Division, Office of Basic Energy Sciences, US Department of Energy. Work at Stanford was supported by the Department of Energy, Office of Basic Energy Sciences, under contract DE-AC02-76SF00515.

References

[1] Shastry B S and Sutherland B 1981 *Phys. Rev. Lett.* **47** 964
[2] Haldane F D M 1982 *Phys. Rev.* B **25** 4925
[3] Noodleman L 1981 *J. Chem. Phys.* **74** 5737
[4] Tamura M, Nakao A and Kato R 2006 *J. Phys. Soc. Japan* **75** 093701
[5] Giamarchi T, Rüegg Ch and Tchernyshyov O 2008 *Nature Phys.* **4** 198
[6] Stone M B, Broholm C, Reich D H, Tchernyshyov O, Vorderwisch P and Harrison N 2006 *Phys. Rev. Lett.* **96** 257203
[7] Zheludev A, Garlea V O, Masuda T, Manaka H, Regnault L-P, Ressouche E, Grenier B, Chung J-H, Qiu Y, Habicht K, Kiefer K and Boehm M 2007 *Phys. Rev.* B **76** 054450
[8] Leuenberger B, Güdel H U and Kjems J K 1985 *J. Magn. Magn. Mater.* **53** 175
[9] Rüegg Ch, Normand B, Matsumoto M, Furrer A, McMorrow D F, Krämer K W, Güdel H-U, Gvasaliya S, Mutka H and Boehm M 2008 *Phys. Rev. Lett.* **100** 205701
[10] Tanaka H, Goto K, Fujisawa M, Ono T and Uwatoko Y 2003 *Physica* B **329–333** 697
[11] Hong T, Garlea V O, Zheludev A, Fernandez-Baca J A, Manaka H, Chang S, Leao J B and Poulton S J 2008 *Phys. Rev.* B **78** 224409
[12] Masuda T, Fujioka A, Uchiyama Y, Tsukada I and Uchinokura K 1998 *Phys. Rev. Lett.* **80** 4566
[13] Regnault L P, Renard J P, Dhalenne G and Revcolevschi A 1995 *Europhys. Lett.* **32** 579
Sasago Y, Koide N, Uchinokura K, Martin M C, Hase M, Hirota K and Shirane G 1996 *Phys. Rev.* B **54** R6835
Martin M C, Hase M, Hirota K, Shirane G, Sasago Y, Koide N and Uchinokura K 1997 *Phys. Rev.* B **56** 3173
[14] Masuda T, Tsukada I, Uchinokura K, Wang Y J, Kiryukhin V and Birgeneau R J 2000 *Phys. Rev.* B **61** 4103
[15] Waki T, Itoh Y, Michioka C, Yoshimura K and Kato M 2006 *Phys. Rev.* B **73** 064419
[16] Oseroff S B, Cheong S-W, Aktas B, Hundley M F, Fisk Z and Rupp L W Jr 1995 *Phys. Rev. Lett.* **74** 1450
[17] Azuma M, Fujishiro Y, Takano M, Nohara M and Takagi H 1997 *Phys. Rev.* B **55** R8658

[18] Uchiyama Y, Sasago Y, Tsukada I, Uchinokura K, Zheludev A, Hayashi T, Miura N and Boni P 1999 *Phys. Rev. Lett.* **83** 632
[19] Oosawa A, Ono T and Tanaka H 2002 *Phys. Rev.* B **66** 020405
[20] Mikeska H-J, Ghosh A and Kolezhuk A K 2004 *Phys. Rev. Lett.* **93** 217204
[21] Bobroff J, Laflorencie N, Alexander L K, Mahajan A V, Koteswararao B and Mendels P 2009 *Phys. Rev. Lett.* **103** 047201
[22] Wessel S, Normand B, Sigrist M and Haas S 2001 *Phys. Rev. Lett.* **86** 1086
[23] Weller M T and Skinner S J 1999 *Acta Crystallogr.* C **C55** 154
[24] Stone M B, Lumsden M D, Chang S, Samulon E C, Batista C D and Fisher I R 2008 *Phys. Rev. Lett.* **100** 237201
[25] Tsujii H, Andraka B, Uchida M, Tanaka H and Takano Y 2005 *Phys. Rev.* B **72** 214434
[26] Samulon E C, Al-Hassanieh K A, Jo Y-J, Shapiro M C, Balicas L, Batista C D and Fisher I R 2010 *Phys. Rev.* B **81** 104421
[27] Uchida M, Tanaka H, Mitamura H, Ishikawa F and Goto T 2002 *Phys. Rev.* B **66** 054429
[28] Stone M B, Lumsden M D, Qiu Y, Samulon E C, Batista C D and Fisher I R 2008 *Phys. Rev.* B **77** 134406
[29] Stone M B, Lumsden M D, Chang S, Samulon E C, Batista C D and Fisher I R 2008 *Phys. Rev. Lett.* **105** 169901(E)
[30] Xu B, Wang H-T and Wang Y 2008 *Phys. Rev.* B **77** 014401
[31] Samulon E C, Shapiro M C and Fisher I R 2011 *Phys. Rev.* B **84** 054417
[32] Oosawa A, Fujisawa M, Kakurai K and Tanaka H 2003 *Phys. Rev.* B **67** 184424
[33] Azuma M, Takano M and Eccleston R S 1998 *J. Phys. Soc. Japan* **67** 740
[34] Larson A C and VonDreele R B 2004 *Los Alamos National Laboratory Report* LAUR 86-748
[35] Mugavero S J III, Bharathy M, McAlum J and zur Loye H C 2008 *Solid State Sci.* **10** 370
[36] Liu G and Greedan J E 1994 *J. Solid State Chem.* **110** 274
[37] Kageyama H, Yoshimura K, Stern R, Mushnikov N V, Onizuka K, Kato M, Kosuge K, Slichter C P, Goto T and Ueda Y 1999 *Phys. Rev. Lett.* **82** 3168
[38] Miyahara S and Ueda K 1999 *Phys. Rev. Lett.* **82** 3701
[39] Haravifard S, Dunsiger S R, El Shawish S, Gaulin B D, Dabkowska H A, Telling M T F, Perring T G and Bonca J 2006 *Phys. Rev. Lett.* **97** 247206
[40] Aczel A A *et al* 2007 *Phys. Rev.* B **76** 214427
[41] Shawish S E and Bonča J 2006 *Phys. Rev.* B **74** 174420
[42] Capponi S, Poiblanc D and Mila F 2009 *Phys. Rev.* B **80** 094407
[43] Manna S, Majumder S and De S K 2009 *J. Phys.: Condens. Matter* **21** 236005
[44] Ma S K, Dasgupta C and Hu C-K 1979 *Phys. Rev. Lett.* **43** 1434
[45] Bhatt R N and Lee P A 1982 *Phys. Rev. Lett.* **48** 344
[46] Fisher D S 1994 *Phys. Rev.* B **50** 3799
[47] Kirkpatrick T R and Belitz D 1996 *Phys. Rev. Lett.* **76** 2571
[48] Beach K S D *March Mtg of the American Physical Society* http://meetings.aps.org/link/BAPS.2010.MAR.Y30.6
[49] Ehlers G, Podlesnyak A A, Niedziela J L, Iverson E B and Sokol P E 2011 *Rev. Sci. Instrum.* **82** 085108